On-Line Self-Calibrating Single Crystal Sapphire Optical Sensor Instrumentation for Accurate and Reliable Coal Gasifier Temperature Measurement

Semi-Annual Technical Progress Report

Reporting Period Start Date: 1 October 2002
Reporting Period End Date: 31 March 2003

Principal Authors: Kristie Cooper, Gary Pickrell and Anbo Wang

Report Issued: April 2003

DOE Award Number: DE-FC-99FT40685

Submitted by: Center for Photonics Technology
Bradley Department of Electrical Engineering
Virginia Polytechnic Institute & State University
Blacksburg, VA 24061-0111

CPT
CENTER FOR PHOTONICS TECHNOLOGY

Disclaimer:

Abstract

This report summarizes technical progress over the first six months of the Phase II program "On-Line Self-Calibrating Single Crystal Sapphire Optical Sensor Instrumentation for Accurate and Reliable Coal Gasifier Temperature Measurement", funded by the Federal Energy Technology Center of the U.S. Department of Energy, and performed by the Center for Photonics Technology of the Bradley Department of Electrical and Computer Engineering at Virginia Tech.

The outcome of the first phase of this program was the selection of broadband polarimetric differential interferometry (BPDI) for further prototype instrumentation development. This approach is based on the measurement of the optical path difference (OPD) between two orthogonally polarized light beams in a single-crystal sapphire disk. The objective of this program is to bring the BPDI sensor technology, which has already been demonstrated in the laboratory, to a level where the sensor can be deployed in the harsh industrial environments and will become commercially viable.

Research efforts were focused on analyzing and testing factors that impact performance degradation of the initially designed sensor prototype, including sensing element movement within the sensing probe and optical signal quality degradation. Based these results, a new version of the sensing system was designed by combining the sapphire disk sensing element and the single crystal zirconia right angle light reflector into one novel single crystal sapphire right angle prism. The new sensor prototype was tested up to 1650ºC.

Table of Contents

List of Figures

1.0 Introduction

In the first phase of this program, five different optical temperature sensing schemes were thoroughly investigated to determine an optimal approach for high temperature measurement in coal gasification systems. Based on comparative evaluation and analysis of the experimental results, the broadband polarimetric differential interferometry (BPDI) was chosen for further prototype instrumentation development. This approach is based on the self-calibrating measurement of the optical path difference (OPD), *i.e.* phase retardation between the two orthogonally polarized light beams in a single-crystal sapphire disk, which is a function of both the temperature dependent birefringence and the temperature dependent dimensional sizes.

In the past half-year, efforts were focused on developing a field ready prototype of the optical sensor for high temperature measurements in the coal gasifier. Detailed theoretical analysis and experimental tests were carried out to study mechanical assembly tolerances and optical signal degradation effects on the temperature measurements. Based on those results, a new version of the sensing probe was designed. The mechanical structure of this new probe was simplified by combining the sapphire-disk sensing element and single crystal zirconia right angle light reflector together into one novel single crystal sapphire right angle prism. This sapphire prism functions as both the sensing element and the light reflector. With fewer optical components in the sensing probe, the mechanical stability was increased, optical power losses in the sensing probe were decreased by eliminating the optical surfaces associated with the extra optical component, and the total cost of the sensing probe was also reduced, which is highly desirable for commercialization.

2.0 Executive Summary

This report summarizes the technical progress over the first six months of the Phase II program "On-Line Self-Calibrating Single Crystal Sapphire Optical Sensor Instrumentation for Accurate and Reliable Coal Gasifier Temperature Measurement", funded by the Federal Energy Technology Center of the U.S. Department of Energy, and performed by the Center for Photonics Technology of the Bradley Department of Electrical and Computer Engineering at Virginia Tech.

During the reporting period, research efforts under the program were focused on the following.

- Analysis of the effect of sensing element rotation within a plane normal to the light propagation direction.

The working principle for the BPDI technology is the detection of the optical path difference (OPD) between two orthogonally polarized light beams in a single-crystal sapphire disk, which is a function of both the temperature dependent birefringence and the temperature dependent dimensional changes. The alignment angle α between the input light polarization direction and directions of principal axes in the sensing element will determine the visibility of the interferogram of the two polarized beams ($\gamma = \sin^2 2\alpha$). Experiments demonstrated that temperature could be measured with the changes in angle α up to 15º. This large angle tolerance can easily be met in the laboratory environment as well as in industrial environments.

- Analysis of the effect of sensing element rotation outside a plane normal to the light propagation direction

  Single crystal sapphire is a uniaxial crystal; one principal refractive index is different from the other two. For non-perpendicular incident light, the birefringence $\Delta n = n_o - n_e$ will be incident angle dependent, because both n_e and the optical path length d that the light passes through are dependent on the incident angle in the birefringent crystal. To completely evaluate the performance of the sensing system for temperature measurements, the dependence of the temperature measurement on light incident angle θ was evaluated. For rotation about the c-axis, the effect on temperature measurements was shown to be less than 4ºC for rotation angles up to 5º; for rotation about the fast axis, the effect was less than 3ºC for rotation angles up to 5º, and less than 2ºC for rotation about the axis at 45º relative to the slow and fast axes for rotation angles up to 5º. To prevent rotation of the sensing element due to mechanical vibration, the sensing element should be held tightly by a single crystal sapphire holder in order to guarantee the same coefficient of thermal expansion (CTE) in the holder and element.

- Analysis of the effect of optical signal quality on temperature measurements

  To evaluate the self-compensating capability of this optical temperature measurement system, the output temperature variations were monitored when the optical source power was varied. The temperature variation range was limited to ±0.45ºC for total optical power changes up to 90%. When the multimode fiber was bent to change the fiber attenuation, the temperature variation was in the range of ±0.4ºC for fiber attenuation up to 9 dB.

- Design of a new, simplified version of the sensor structure

  Based on sensor performance testing results, a new version of the sensing system was designed by combining the sapphire disk sensing element and the single crystal zirconia right angle light reflector together into one novel single crystal sapphire right angle prism. The mechanical structure is simplified and stability increased in this new sensing probe, which is a major step toward scaling up the sensor system for a full field demonstration at Global Energy Technology's Wabash River Facility.

- Testing of the new sensor structure up to 1650ºC

  With a single crystal sapphire right angle prism as the sensing element, the temperature sensor achieved a wide dynamic range over 1600ºC with high accuracy. Its resolution and accuracy are comparable to commercially available B-type thermocouples. Further resolution improvement can be achieved by changing the sensing element sizes.

Efforts during the coming months will focus on further laboratory testing and calibration of the newly revised sensor version, field ready sensor prototype design, and site preparation and installation for the gasifier field test.

3.0 Theory of Sensor Operation

To illustrate the working principle of the BPDI sensing system, analysis of the sensor mechanical structure and optical signal degradation effects are described briefly as follows. As shown in Figure 3.1, the broadband light from a high power light emitting diode is injected into a multimode optical fiber and propagates through a two by two fiber coupler to the sensor head. The light is first converted into a linearly polarized collimated optical beam and travels across a free space enclosed by a high temperature ceramic tube and a single crystal sapphire tube to a single crystal sapphire disk, functioning as the sensing element. The sapphire disk is arranged such that the linear polarization is at 45º with respect to the fast and slow axes of the crystal. After passing through the sapphire disk, the two linear polarization components along the fast and slow axes experience a differential phase delay due to the sapphire birefringence. The light, containing the two different linear polarization components, is then reflected by a right angle zirconia prism and passes through the sapphire sensing element again, so the differential phase retardation is doubled. The two linear components with a differential phase delay are then combined along the polarizer direction to interfere with each other. The light is then collected by the same input optical fiber and travels back along the same fiber and through the same coupler to the optical detection end. The returned light intensity can be expressed as

$$I(\lambda) = 2kI_S(\lambda)\left(1+\cos\left(\frac{2\pi d(T)\Delta n(T)}{\lambda}\right)\right), \qquad \textbf{(3-1)}$$

where $I_S(\lambda)$ is the spectral power distribution which is a function of the wavelength (λ) of the broadband light source; k is a parameter describing the power loss of the optical system, and can be treated as a constant; d is the thickness of the sapphire disk; and $\Delta n = n_o - n_e$ is the birefringence of the sapphire disk. Both d and Δn are functions of the temperature T. From this equation, it can be seen that the output spectral density is a function of the light wavelength and the differential phase delay, which is a function of temperature. It is therefore possible to extract the temperature information by measuring the output optical spectrum.

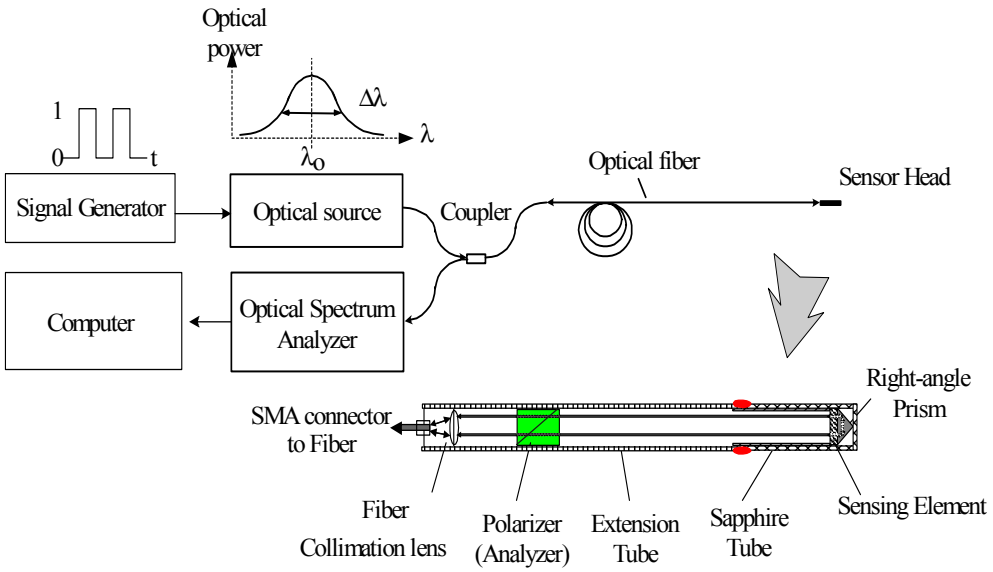

Figure 3.1. Schematic of the single-crystal sapphire based optical high temperature sensor.

Based on the BPDI technology, a complete prototype sensor instrumentation system was designed and implemented to demonstrate the technical feasibility of the sensor technology for reliable and accurate high temperature measurement.

4.0 System Performance Optimization

Research efforts were focused on analyzing and testing the performance degradation factors of the initially designed sensor prototype. Those factors include the effects of the sensing element movement within the sensing probe and optical signal quality degradation. Additional factors will be analyzed in the future in order to optimize its performance.

4.1 Effect of Sensing Element Rotation Within a Plane Normal to the Light Propagation Direction

The results shown in Equation 3-1 assume the polarization direction *P* of the input light beam is at 45º relative to both the fast- and slow-axis of the sensing element in the plane normal to the light propagation direction, as shown in Figure 4.1 (α=45º). It is difficult to align all optical components accurately during the experimental setup. Also, mechanical vibration may change the relative position between the sensing element and polarizer during both setup and operation. Therefore, the cases for an angle $\alpha \neq 45º$ are common. Before assembling and sealing all optical components to form the solid sensing probe, one necessary task is to analyze the dependence of the temperature measurement accuracy on the angle α.

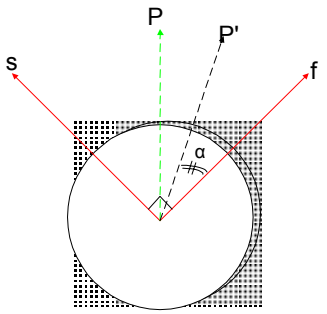

Figure 4.1. Misalignment between the optical polarizer and the sensing element.

When a linearly polarized light beam passes through the sapphire sensing element, the light behaves as if it is divided along the x and y directions separately as shown in Figure 4.2. Along the x-axis the refractive index will be n_e. Along the y-axis the refractive index will be n_o. At the input surface of the sapphire sensing element, the ordinary wave and extraordinary wave are still in phase, *i.e.* the phase difference δ=0. After the light passes through the sensing element , the phase difference δ will change from zero to

$$\delta = 2\pi d\Delta n / \lambda \,, \qquad \textbf{(4-1)}$$

where d is the thickness of sensing element, $\Delta n = n_o - n_e$ is the birefringence, and λ is the optical wavelength. Depending on the magnitude of δ, and the alignment angle α between the input light polarization direction and directions of the principal axes in the sensing element, the output light from the sensing element can be linearly polarized, circularly polarized or elliptically polarized light.

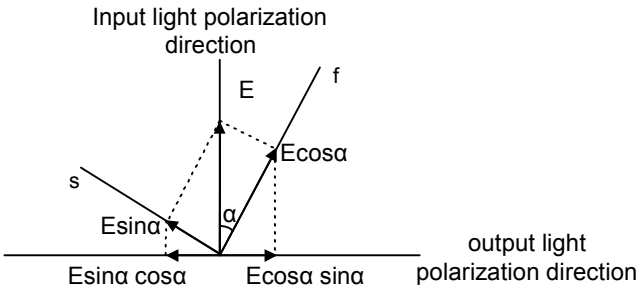

Figure 4.2. Decomposition of the linearly polarized input light.

If another linear polarization analyzer is placed behind the sensing element with its polarization direction perpendicular to the original input light polarization direction, the electrical field of the output optical wave can be expressed in vector form as

$$\vec{E}_{out} = \vec{E}_0 \sin\alpha\cos\alpha + \vec{E}_0 \sin\alpha\cos\alpha \,, \qquad \textbf{(4-2)}$$

where $\bar{E}_{out}$, $\bar{E}_0 \sin\alpha\cos\alpha$ and $\bar{E}_0 \sin\alpha\cos\alpha$ are all vectors, and the intensity of the output light will be:

$$I_{out} = |E_{out}|^2 . \qquad \textbf{(4-3)}$$

The results will contain the information about δ, which is the result of interference between two polarized beams:

$$\begin{aligned} I_{out} &= (E_0 \frac{\sin 2\alpha}{2})^2 + (E_0 \frac{\sin 2\alpha}{2})^2 + 2E_0^2 (\frac{\sin 2\alpha}{2})^2 \cos\delta \\ &= I_0 (\frac{\sin 2\alpha}{2})^2 (2 + 2\cos\delta) \\ &= I_0 (\sin 2\alpha)^2 \cos^2(\frac{\delta}{2}) \end{aligned} \qquad \textbf{(4-4)}$$

From Eq.(4-2), δ is a function of the product $d\Delta n$; when the temperature changes, the thickness d of the sapphire sensing element will change, and $\Delta n = n_o - n_e$ will also change. Eq.(4-4) is thus a function of temperature.

The factor related to angle α in Eq.(4-4) will determine the visibility of the interferogram of the two polarized beams. After normalization by dividing the input broadband optical source $I_0(\lambda)$, whose spectral curve can be approximated as a Gaussian profile, by the measured spectrum curve $I(\lambda)$, the visibility of the interferogram will be

$$\gamma = \sin^2 2\alpha . \qquad \textbf{(4-5)}$$

The dependence of the visibility on the angle α is plotted in Figure 4.3(a).

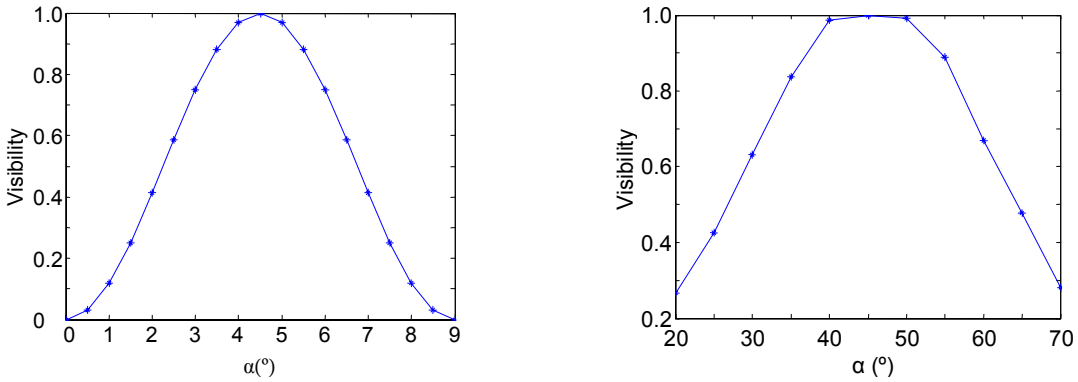

(a) Theoretical simulation results **(b) Experimental tests results**

Figure 4.3. Visibilities dependence on the angle α between the light polarization direction and birefringence axes of the sensing element

As shown in Figure 4.3(b), the measured visibility of the interferogram is dependent on the angle α, as predicted by Figure 4.3(a). The visibility is about 1 when α=45°, and decreases for angles smaller than 45°, or increases for values larger than 45°. To calculate the phase delay

generated in the sensing elements as a result of the surrounding temperature, a minimum visibility is required for the interferogram. Therefore there is a minimum requirement on the alignment angle α. The ideal angle is 45º, which corresponds to a visibility of 1.

Figure 4.4 shows that even for different visibility values, the peaks and valleys (corresponding to the maximum and minimum intensity of the measured spectral curves) are fixed. According to Eq.(4-1), only these peaks and valleys are used to extract temperature information; accurate temperature measurements are still achievable as long as the visibility is maintained above a threshold value. The experimental results demonstrate that temperature can be measured with the change in angle α up to 15º, as shown in Figure 4.4. This wide angle tolerance can be easily met in the laboratory environment as well as in the industrial environments. Thus the requirements on mechanical design are relieved.

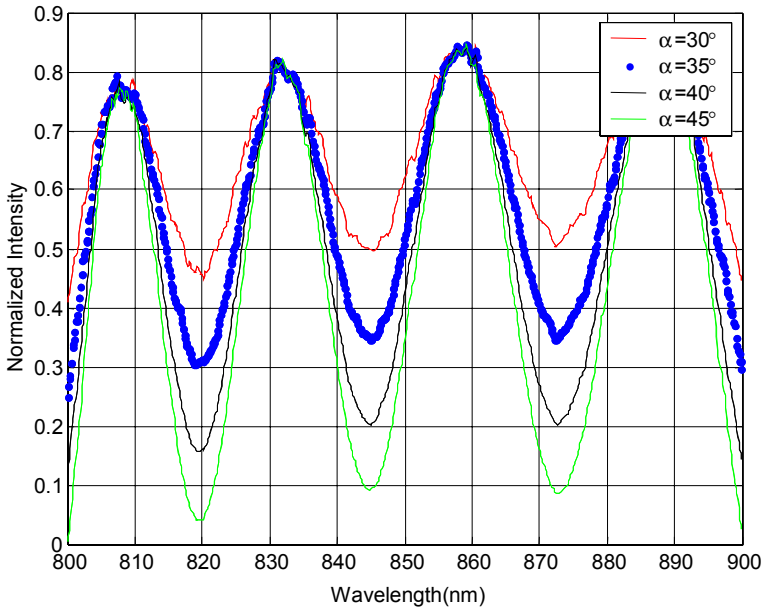

Figure 4.4. Experimental interferograms with different angle α.

4.2 Effect of Sensing Element Rotation Outside a Plane Normal to the Light Propagation Direction

As presented in Chapter 3.0, the working principle for this BPDI technology is the detection of the optical path difference (OPD), *i.e.* the phase retardation between the two orthogonally polarized light beams in a single-crystal sapphire disk, which is a function of both the temperature dependent birefringence and the temperature dependent dimensional sizes. The retardation in the sensing element is actually a refractive index effect. As light passes from a vacuum into a material, the speed of light is reduced by a factor that is the reciprocal of the refractive index. If a body retards all polarizations to the same degree, *i.e.* independent of propagation direction, the body is said to be isotropic. On the other hand, if the refractive

index and retardation depends on the polarization form and direction of propagation, the body is called anisotropic. An anisotropic material is completely characterized by three principal refractive indices, which can be represented by an index ellipsoid. In uniaxial materials, one principal refractive index is different from the other two. The rays that are used to define the unique (optic) axis are called ordinary rays and the refractive index is called n_o. Those that are associated with the other axes are called extraordinary rays and the refractive index is called n_e. Materials with different principal refractive indices are therefore referred to as birefringent.

As shown in Figure 4.5, the index ellipsoid is used mainly to determine the magnitude of the two indices of the refraction (n_o and n_e corresponding to D1 and D2) for the two orthogonally polarized beams, as well as the corresponding directions of D associated with the two independent light waves that can propagate along an arbitrary direction, *s,* in a crystal. This is done by finding the intersection ellipse between a plane through the origin that is normal to the direction of light propagation, *s,* and the index ellipsoid with axes D1 and D2. The axes of the intersection ellipse are equal in length to $2n_o$ and $2n_e$, where n_o and n_e are the indices of refraction for the two orthogonally polarized light waves. The beams are polarized in directions parallel to D1 and D2.

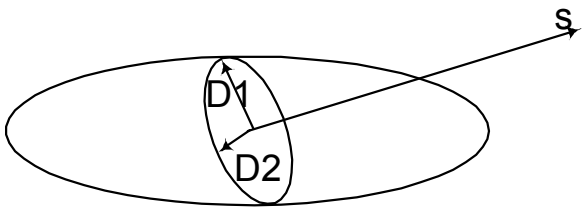

Figure 4.5. Method of the index ellipsoid to determine the refractive indices of lights propagating along s direction.

Single crystal sapphire is a uniaxial crystal because of its hexagonal crystalline structure, shown in Figure 4.6(a). The index ellipsoid corresponding to the hexagonal inner atomic structure is shown in Figure 4.6(b). The refractive index along the c-axis is n_o, the refractive index along the a-axis is n_e. Single crystal sapphire is a negative uniaxial crystal, meaning $n_o > n_e$; the c-axis is the slow axis and the a-axis is the fast axis. In the single crystal sapphire shown in Figure 4.6, the refractive index is a constant for all directions of propagation in the x-y plane. There is no birefringence in this plane, called the C-plane. In the y-z or x-z plane, the refractive indices along different axes are different; birefringence $\Delta n = n_o - n_e$ exists. To utilize the inherent birefringence of the crystal, an A-plane cut sapphire crystal is used as a sensing element. With the propagation direction of the incident light wave perpendicular to the sapphire sensing disk surface (A-plane), the phase delay between the two orthogonally polarized beams will be $\delta = 2\pi d\Delta n/\lambda$, where d and Δn are the only terms that are a function of temperature. Therefore temperature can be measured directly by monitoring the phase delay δ with BPDI technology. For the case of non-perpendicular incident light, the birefringence $\Delta n = n_o - n_e$ will be incident angle dependent, because both n_e and the optical path length d that the light passes through are dependent on the incident angle in the birefringent crystal. Thus a more general formula for the phase delay should be:

$$\delta(T,\theta)=\frac{2\pi d(T,\theta)\Delta n(T,\theta)}{\lambda}, \qquad (4\text{-}6)$$

where T is the temperature, and θ is the light incident angle.

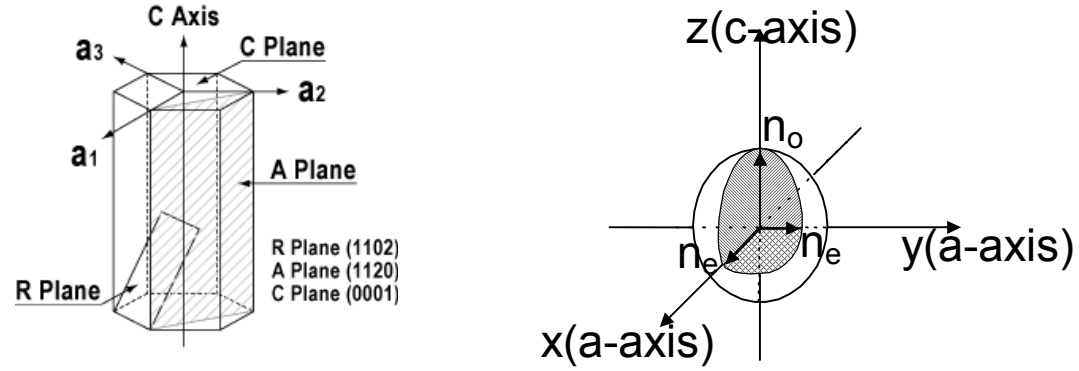

(a) Hexagonal crystalline structure (b) Index ellipsoid

Figure 4.6. The refractive index ellipsoid for single crystal sapphire.

To completely evaluate the performance of the sensing system, the dependence of the temperature measurement on the light incident angle θ must be considered. Based on the discussion of the index ellipsoid of the single crystal sapphire, refractive indices for arbitrary light propagating in the crystal can be determined by the intersection ellipse; the lengths of the short and long axis of the intersection ellipse are related to the refractive indices along fast-axis and slow-axis. These two axes can fully characterize the entire refractive index ellipse. Thus rotation along the fast axis and slow axis can be used to analyze more general situations for rotation along other directions in detail by combining the results for these two special cases.

4.2.1 Rotation about the slow-axis (i.e. c-axis):

As shown in Figure 4.7(b), the refractive indices for the ordinary and extraordinary waves are all constant, thus the birefringence $\Delta n = n_o - n_e$ is independent of the light incident angle. For this situation, the optical path d, along which light passes through the sapphire disk, is the only factor that is incident angle dependent.

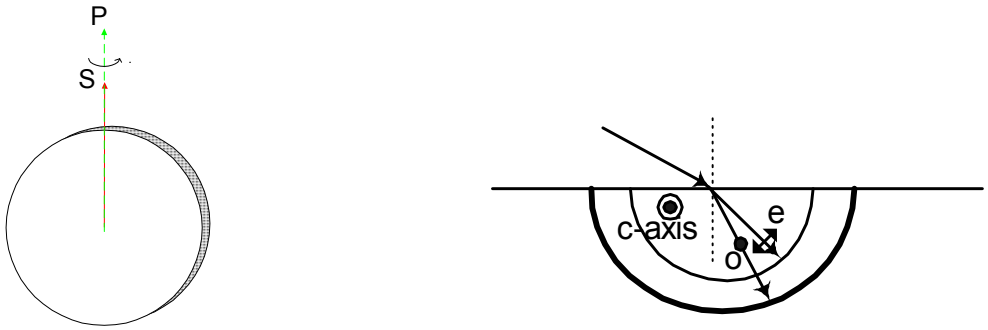

(a) **(b)**

Figure 4.7. (a) Rotation along s-axis of sensing element; (b) Wave vectors for double refraction in sapphire, with the optic axis parallel to the boundary and perpendicular to the plane of the incidence.

In the room temperature environment, the refractive indices of single crystal sapphire can be approximated as the following, plotted in Figure 4.8(a).

$$n_o^2 - 1 = \frac{1.4313493\lambda^2}{\lambda^2 - 0.0726631^2} + \frac{0.65054713\lambda^2}{\lambda^2 - 0.1193242^2} + \frac{5.3414021\lambda^2}{\lambda^2 - 18.028251^2}$$
$$n_e^2 - 1 = \frac{1.5039759\lambda^2}{\lambda^2 - 0.0740288^2} + \frac{0.55069141\lambda^2}{\lambda^2 - 0.1216529^2} + \frac{6.5927379\lambda^2}{\lambda^2 - 20.072248^2} \quad \textit{(4-7)}$$

The birefringence $\Delta n = n_o - n_e$ is also plotted in Figure 4.8(b) as a function of wavelength.

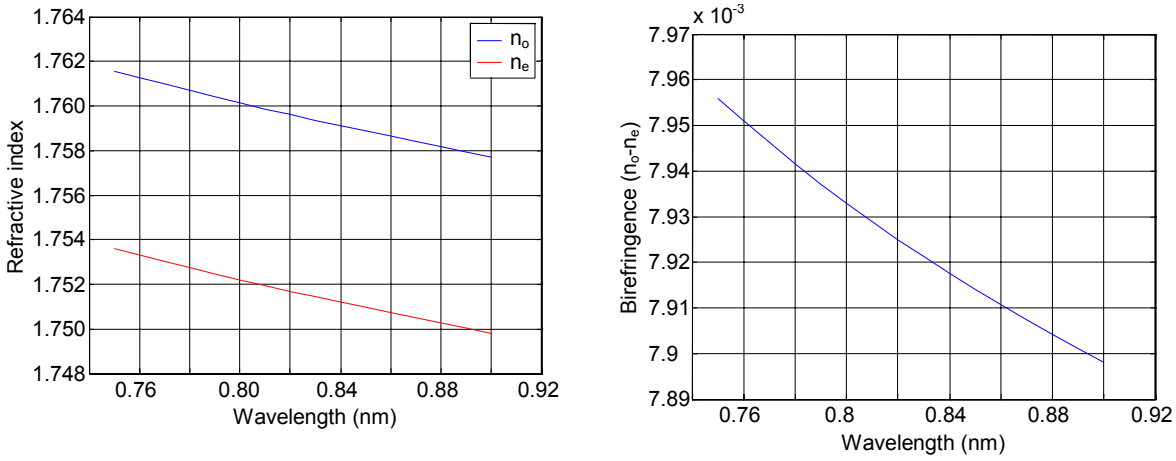

(a) **(b)**

Figure 4.8. Refractive indices vs. wavelength (a) and birefringence (b) for sapphire.

Selecting the refractive indices values at the wavelength of interest λ=850nm, n_e=*1.751* and n_o=*1.7589*, the refraction angles vs. incident angle for the ordinary and extraordinary waves are plotted in Figure 4.9(a). The difference between the two angles is very small (Figure 4.9(b) and they can be approximated as equal in the analysis of rotation effects on the temperature measurement. The OPD change is only related to changes in *d* as a result of the disk rotation. As shown in Figure 4.10(a), the OPD value is *d* with normal incident light, and *d'* with the sensing disk rotated an angle θ_0.

$$d = (n_o - n_e)L;$$
$$d' = (n_o - n_e)L/\cos\theta_1 \quad \textit{(4-8)}$$

where θ_1 is the refraction angle related to the incident angle θ_0. Changes of OPD vs. rotation angles (θ_0) up to 50º have been tested; the results are compared with theoretical results in Figure 4.11.

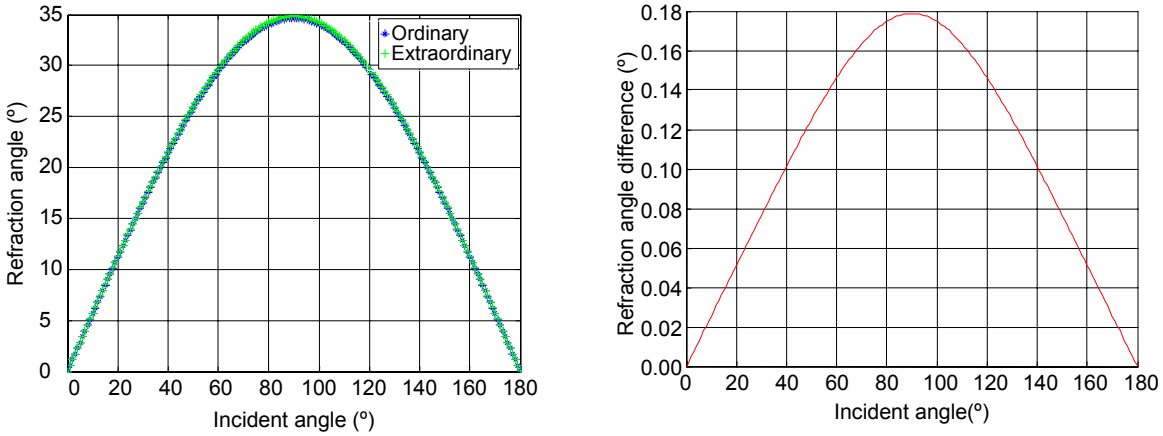

(a) (b)

Figure 4.9. Refraction angles of the ordinary and extraordinary waves (a) and the difference between the two (b).

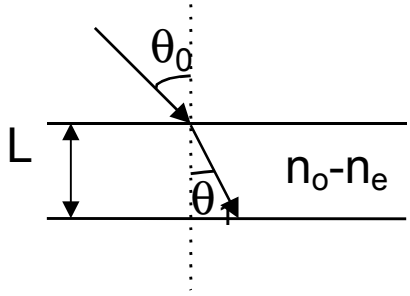

Figure 4.10. Sensing element rotation effect on the optical path difference (OPD).

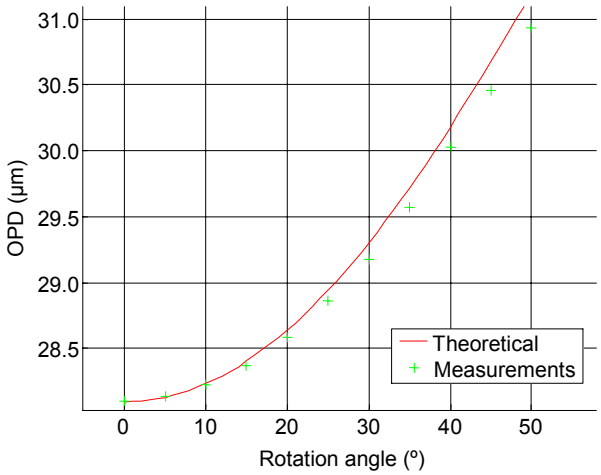

Figure 4.11. Sensing element rotation effects along s-axis on the OPD measurements.

In both the theoretical analysis and experimental tests, it was demonstrated that the OPD values increase with increasing rotation angles about the c-axis. In a constant temperature environment, if the sensing element rotates, the OPD values change rather than remaining constant to indicate a constant temperature value. This change in OPD values will thus affect the temperature measurement accuracy. If the sensing element remains at the same position without rotation during the entire measurement process, the measured temperature is accurate. The rotation may be caused by mechanical vibration or permanent rotation. To prevent rotation of sensing element due to mechanical vibration, the sensing element should be held tightly by the single crystal sapphire holder in order to guarantee the same coefficient of thermal expansion (CTE), so that thermal expansion can be accounted for in when determining the temeprature. For a permanent movement of the sensing element, the sensing probe must be recalibrated for accurate temperature measurements.

Using the OPD/rotation angle curves shown in Figure 4.11, we can estimate the rotation effect on the OPD measurements within a certain rotation angle range, and thus evaluate the rotation effects on the temperature measurements according to the calibrated relationship between the OPDs and temperature values. It has been shown that the effect on temperature measurement is less than 4ºC for rotation angles up to 5º.

4.2.2 Rotation about the fast-axis (i.e. a-axis):

For this case, as shown in Figure 4.12(b), the refractive index is independent of the light incident angle for the normally incident wave in an a-plane sapphire disk. Its value is the ordinary refractive index of the crystal n_o. This wave obeys Snell's law:

$$n_i \sin\theta_0 = n_o \sin\theta_1 \qquad \textbf{(4-9)}$$

where n_i is the index of refraction of the medium from which the light is incident, and θ_0 and θ_i are the incident angle and related refraction angle of the light, respectively.

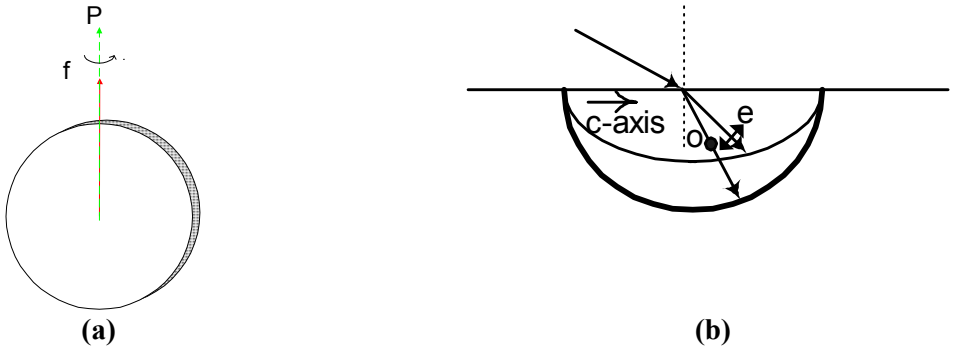

Figure 4.12. (a) Rotation along fast axis of sensing element; (b) Wave vectors for double refraction in sapphire, with the optic axis parallel to the boundary and perpendicular to the plane of incidence.

For extraordinary waves in an a-plane sapphire disk, the corresponding refractive index depends on the direction of light propagation. With rigorous mathematical analysis shown in the appendix, the refraction angle θ_2 and refractive index n_e can be expressed as

$$\theta_2 = \tan^{-1}\left(\sqrt{\frac{{n_o}^2 n^2 \sin^2\theta_0}{{n_{eo}}^2({n_o}^2 - n^2\sin^2\theta_0)}}\right), \qquad \textbf{(4-10)}$$
$$n_e = \frac{{n_{eo}}^2 {n_o}^2 (1+\tan^2(\theta_2))}{{n_{eo}}^2 \tan^2(\theta_2) + {n_o}^2}$$

where n is the refractive index of the media from which the light is incident ($n=1$ for incident light from the air); n_{eo} is a special n_e value for the extraordinary waves when incident light is normal to the surface of the a-plane sapphire disk. Refractive indices for the extraordinary waves increase as the refraction angles increase, as shown in Figure 4.13.

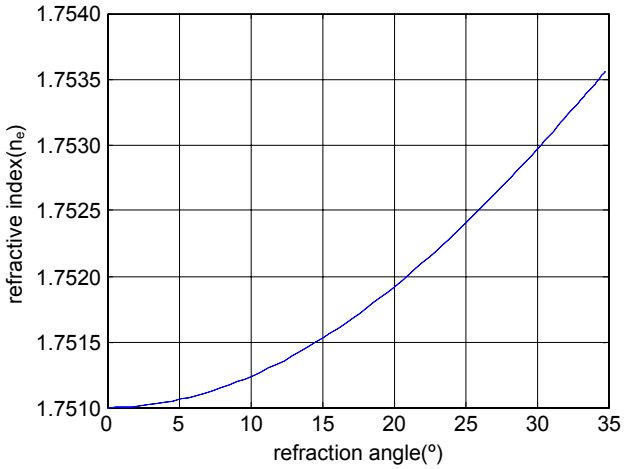

Figure 4.13. Refractive index vs. light incident angle for the extraordinary waves.

Selecting the refractive index values for the wavelength of interest, $\lambda=850nm$ ($n_{eo}=1.751$, $n_o=1.7589$), the refraction angles for the ordinary wave and the extraordinary wave are plotted in Figure 4.14(a). The difference between the two angles is so small, as shown in Figure 4.14(b), that the refraction angles in the sapphire disk for these two waves can be approximated as equal for analysis of the rotation effects on temperature measurements. The change in OPDs is related to the d changes as a result of the disk rotation, as well as the changes in refractive index for the extraordinary wave, as shown in Figure 4.13. The OPD value is a product of the birefringence $\Delta n = n_o - n_e$ and d if the light is normally incident on the sensing element surface, and d' if the sensing disk rotated an angle θ_0, as shown in Figure 4.15.

$$d = (n_o - n_e)L;$$
$$d' = (n_o - n_e)(\theta_2)L/\cos\theta_2 \qquad \textbf{(4-11)}$$

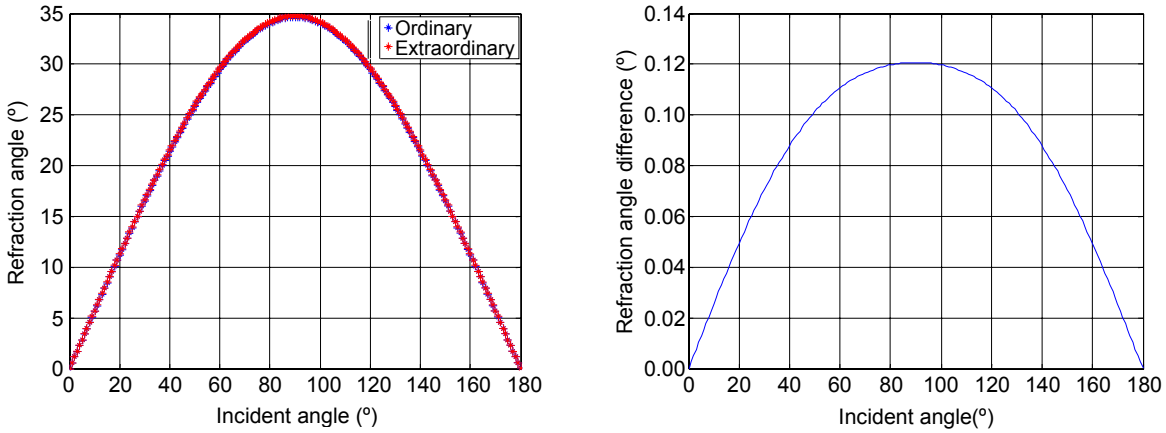

(a) (b)

Figure 4.14. Refraction angles of the ordinary and extraordinary waves (a) and the difference between the two (b).

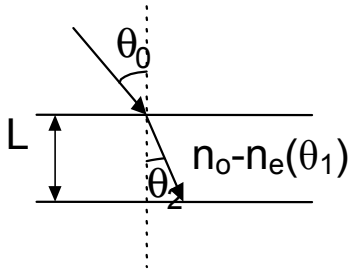

Figure 4.15. Rotation effects on the optical path difference between ordinary wave and extraordinary wave.

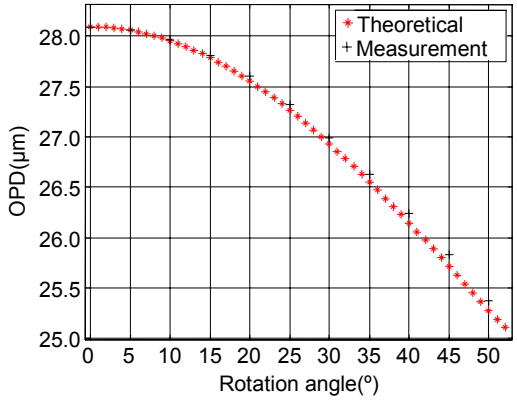

Figure 4.16. Effect of rotation about the f-axis on the OPD measurements.

The change in OPDs vs. rotation angles up to 50º has been tested; the results are compared with theoretical results in Figure 4.16.

According to the theoretical analysis and experimental tests, the OPD values increase when the sensing element rotates about the a-axis. By comparing curves shown in Figure 4.10 and Figure 4.15, it is evident that the magnitude of the OPD change is smaller for rotation about the a-axis than for rotation about the c-axis for a given rotation angle. These results can be explained by following. When the sensing element rotates about the a-axis, the *d* value increases and the birefringence decreases if the light incident angle increases; thus the combined effects cause the OPD to decrease. Because the OPD depends on the position of the sensing element, rotation along the fast axis of the sensing element will affect the temperature measurement accuracy, even though its effect is relatively small compared with the effect generated by rotation along slow axis. The sensing element should be maintained in a fixed position for all measurement processes, without rotation, to ensure accurate temperature measurements. Again, to prevent rotation of sensing element by mechanical vibration, the sensing element should be held tightly by a single crystal sapphire holder in order to provide coefficient of thermal expansion (CTE) matching during temperature changing processes. For permanent movement, the sensing probe must be recalibrated for accurate temperature measurements.

With the relationship between the OPD and rotation angle shown in Figure 4.16, we can estimate the effect of rotation about the fast axis on the OPD measurements within certain rotation angle ranges, and thus evaluate the rotation effects on the temperature measurements based on the calibrated relationship between OPDs and temperature values. It was demonstrated that the effect on temperature measurement is less than 3ºC for rotation angles up to 5º.

4.2.3 Rotation about the axis 45º relative to slow-axis.

According to the analytical and experimental results in the two sections above, it is possible to reduce the dependence of the OPD values on the rotation angle by letting the rotation occur about an axis between the slow axis and fast axis. The total rotation effect on temperature measurements can thus be partially cancelled between the increasing and decreasing values of OPD. We tested the rotation of the sensing element about the z-axis. The direction of this axis is at 45º relative to both the slow axis and fast axis of the sensing element, as shown in Figure 4.17. The polarization direction of the incident optical light is also along z-direction. This rotation can be treated as:

$$OPD(45^{\circ}\ rotation) = OPD(0^{\circ}\ rotation) + OPD(90^{\circ}\ rotation), \qquad \textbf{(4-12)}$$

i.e. partial rotation about fast axis, which will cause the OPDs to decrease, and partial rotation about the slow axis, which will cause the OPDs to increase. Experimental results are shown in Figure 4.18. With small rotation angles (<5º), the effect on the temperature measurement is less than 2ºC, which is determined based on the calibrated relationship between temperature and OPD.

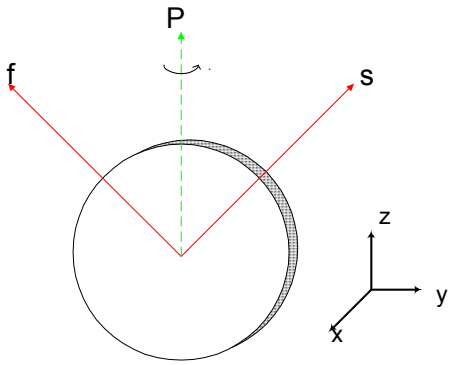

Figure 4.17. Rotation about the 45º axis relative to the s-axis of sensing element.

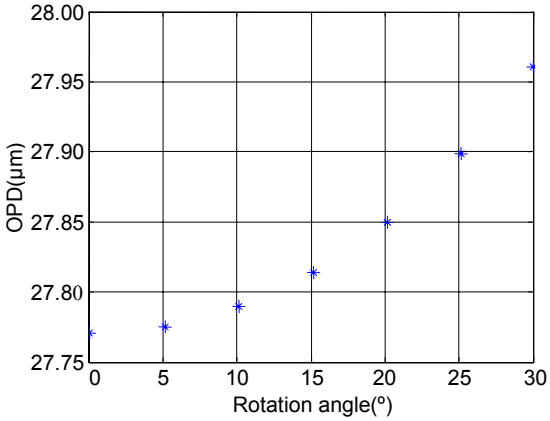

Figure 4.18. Effect on the OPD measurements of rotation about the axis at 45º relative to the f-axis of the sensing element.

4.3 Effect of Optical Signal Quality on Temperature Measurements

The BPDI technology extracts temperature information by absolute measurement of the phase delays between the two orthogonally polarized beams, which is attractive for harsh environment applications because it does not require initialization and/or calibration when the power is switched on. To make the absolute measurement meaningful, self-compensating capability is desired so that the optical power fluctuations and fiber loss changes can be fully compensated.

By self-referencing the two orthogonal polarized beams, the BPDI technology possesses a self-compensating capability. To evaluate the self-compensating capability of this optical temperature measurement system, the output temperature variations were monitored when the optical source power was altered by changing its driving current. Figure 4.19(a) shows the output temperature variations as a function of the normalized optical power of the optical source (LED). As shown, the temperature variation range is limited to ±0.45ºC for total optical power changes up to 90%. Theoretically speaking, changing the driving current of a semiconductor optical source (LED) would also change the spectrum in addition to the

optical power level change and the distortion of the source spectrum would also introduce error into the measurement results through the non-centered filtering effect. Therefore, the measurement results shown in Figure 4.19(a) also indicate the contribution from the source spectrum distortion. To evaluate the self-compensating capability of this optical temperature measurement system, the output temperature variations were also monitored when the multimode fiber was bent to change the fiber attenuation. Figure 4.19(b) shows that the temperature variation is in the range of ±0.4ºC for fiber attenuation up to 9 dB.

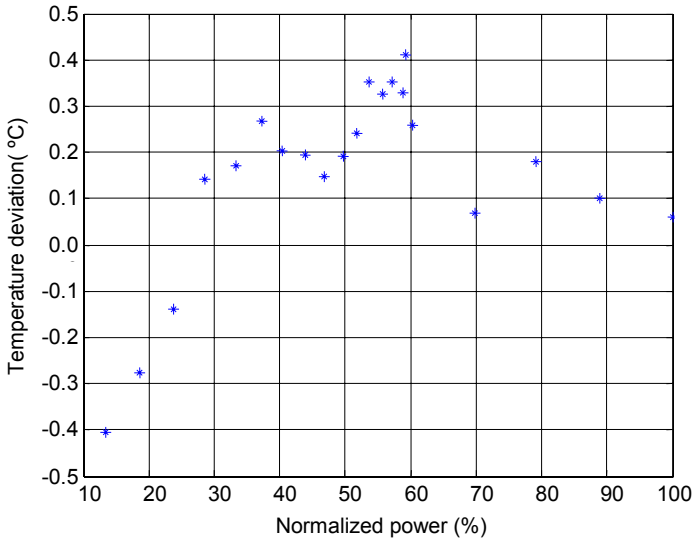

(a)

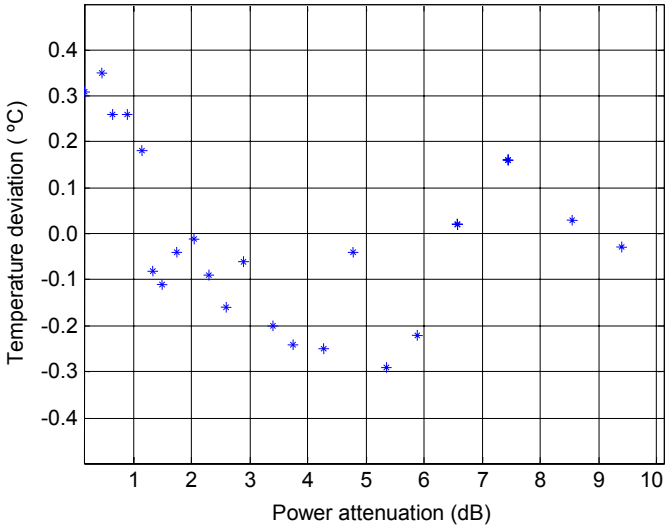

(b)

Figure 4.19. BPDI system measured temperature variations as a function of (a) the normalized optical power and (b) fiber losses.

5.0 New Sensing System Design

Based on the analytical results shown in Section 4.0, a new version of the sensing system with a simplified sensing probe mechanical structure was designed. This new design simplifies the sensing probe structure by combining the sapphire disk sensing element and the single crystal zirconia right angle light reflector together into a single crystal sapphire right angle prism.

5.1 New Sensing Element Design

The previously developed sensing probe prototype utilized both a single crystal sapphire disk as sensing element and a single crystal zirconia prism as the light reflector in the sensing location. These materials do not have the same CTE. This may generate thermal stress for the mechanical packaging, *i.e*. thermal expansion generated instability in high temperature environments. This may also cause an additional optical reflection at the surfaces of the zirconia prism and increase the reflection losses. From a cost minimization standpoint, a single crystal zirconia right angle light reflector is also very expensive. In the new version of the sensing probe, a novel single crystal sapphire right angle prism, functioning as both sensing element and light reflector, is employed. This single crystal sapphire prism possesses a special geometrical structure and crystallographic orientation for those dual functions.

In low temperature environments, a mirror is commonly used as a light reflector. The mirror is usually made by coating one surface of a glass plate with different materials, typically dielectrics and metals. Since those dielectric or metal coatings cannot survive the corrosive environment, either because of the coating materials degrade at high temperature and/or in chemically corrosive environments, or because of CTEs of those materials do not match those of the glass substrate, they cannot function as a mirror in high temperature/corrosive environments. Instead, a right-angle prism is an attractive design since only one material is employed with a special geometrical 90º angle and total-internal reflection is employed to avoid reflection power losses. We used single crystal sapphire to fabricate the right angle prism because of its inertness and high temperature properties.

The single crystal sapphire's inherent birefringence is needed to make the prism function as a sensing element. As shown in Figure 5.1, when light passes through the prism, it will propagate in three different directions. Beam 1 propagates along JC in the +X direction, along CD in the –Y direction, and along DK in the –X direction. Beam 2 propagates along LE in the +X direction, along EF in the –Y direction, and along FM in the –X direction. Different incident light beams encounter different path lengths in different directions. Along Y direction in the prism, beam 1 travels through length CD, while beam 2 travels through EF, which is a different length. We selected the crystallographic orientation of the prism as follows: A-plane as the base of the sapphire prism and both the smaller sides are C-plane, as shown in Figure 5.1(b). With this design, when the light propagates in the x-direction, such as JC and LE, it experiences the birefringence generated by both the a-axis and c-axis. Because of the symmetric inner atomic structure of single crystal sapphire, when the light propagates in the y-direction, such as CD and EF, it also experiences the birefringence

generated by both the a-axis and c-axis. Therefore the total birefringence will be equal and independent of the paths in which optical beams propagate, and independent of the location of incidence on the prism. According to the geometric relationships, all light beams will experience the same length in the prism, equivalent to the length of line AB. Thus the OPD in the prism will be:

$$OPD = |AB|\Delta n . \qquad \textbf{(5-1)}$$

This prism thus functions as a sensing disk with thickness of the length AB as well as a light reflector. Figure 5.2 shows the designed geometrical dimensions of the prism and three pieces of the novel single crystal sapphire prisms.

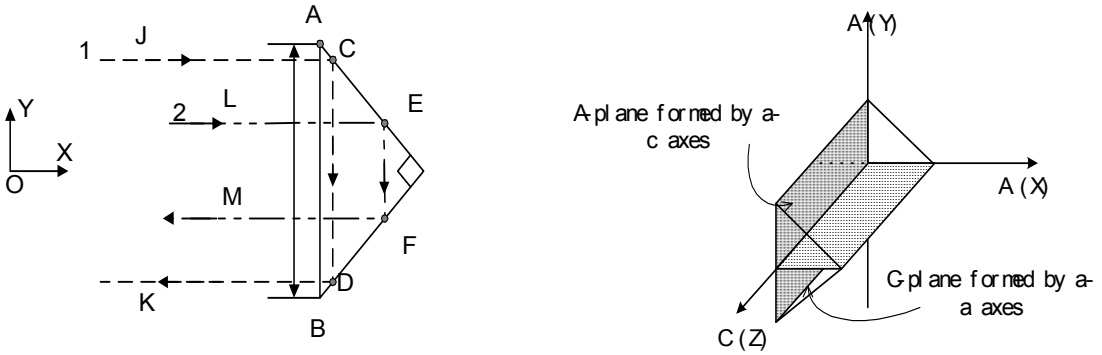

(a) Optical propagation path in the prism **(b) Crystallographic orientation in the prism**

Figure 5.1. Design of the single crystal sapphire right angle prism.

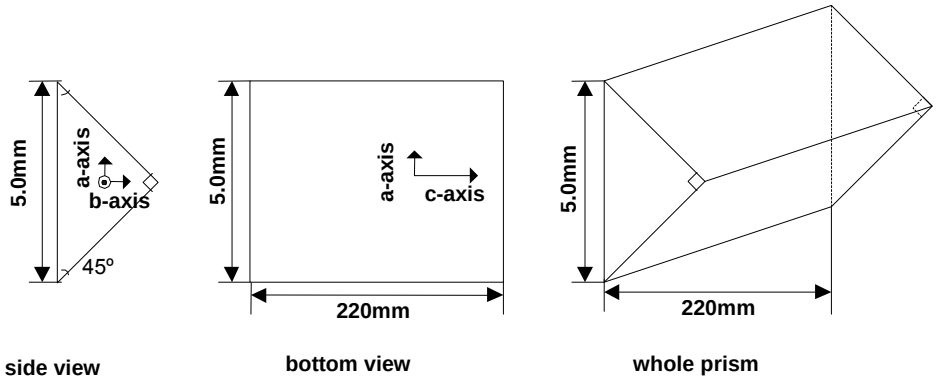

(a) Geometrical sizes of the prism

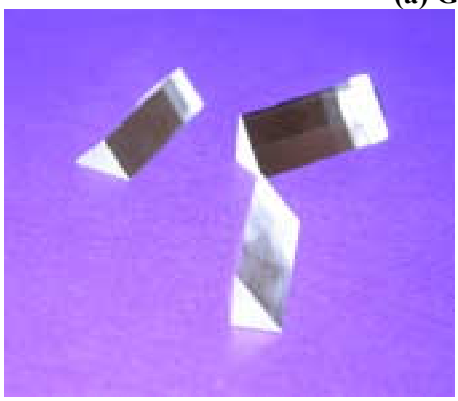

(b) Fabricated single crystal sapphire right angle prisms

Figure 5.2. Single crystal sapphire right angle prism

5.2 New Version of Sensing Probe Structure and System Testing Results

With a single right angle prism at the end of the sensing probe, the mechanical structure of the sensing head is simplified dramatically, as shown in Figure 5.3. The sensing prism is fixed at the end of the inner supporting tube, in which a slot of the correct size to fit the prism is machined. The outer protective sapphire tube covers the inner tube and sensing prism, with a certain amount free space between its end and the sensing prism so that the prism can expand freely at high temperature. An extension tube is necessary at the other end of the sapphire protection tube to avoid thermal damage to the optical fiber collimator and optical polarizer; these components cannot survive high temperature over 200ºC. The total sensing tube will thus be about two meters long together with the extension tube.

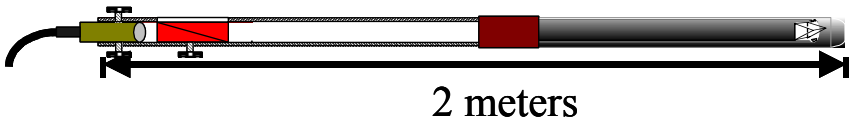

Figure 5.3. Simplified sensing probe assembly.

The new version of the optical high temperature sensing system is shown in Figure 5.4. A broadband light emitting diode (LED) is modulated by a rectangular wave from a signal generator. The pulsed light is guided through a multimode optical fiber into the sensing probe where the optical signal is encoded with temperature information by the sensing prism and reflected back, and then is collected by the same optical fiber and guided back into an optical spectrum analyzer. The optical signal detected not only includes the temperature information carrier (temperature signature), but also some background due to blackbody radiation. Blackbody radiation exists for any material with a temperature above absolute zero and becomes stronger with increased temperature. Its power distribution follows Plank's blackbody radiation law. This blackbody radiation is represented as continuous red lines under the modulated optical pulses shown in Figure 5.4. The modulation scheme used discriminates the temperature information carrier as AC components, and the blackbody radiation as DC components. The DC components can be easily eliminated by utilizing the computational function of the computer.

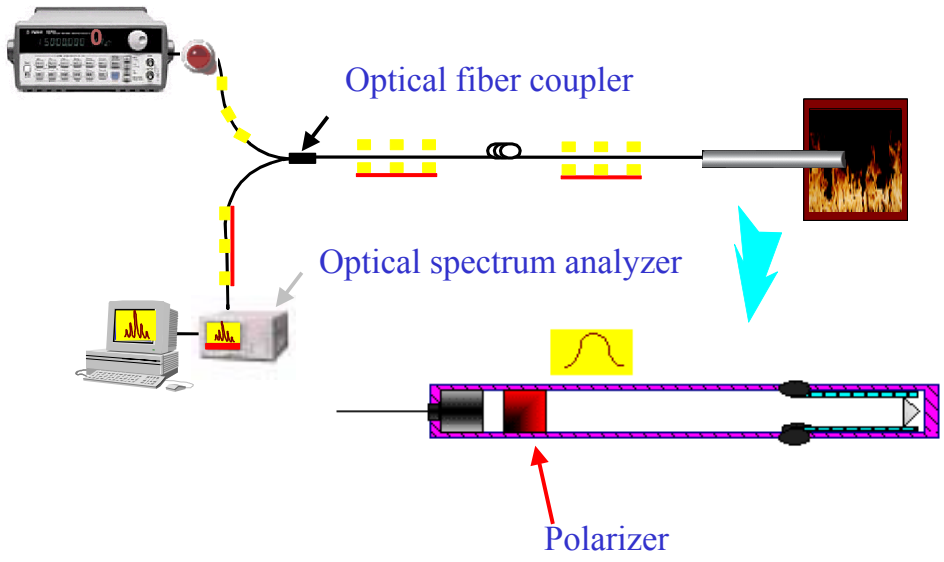

Figure 5.4. Single-crystal sapphire based optical high temperature sensing system.

The performance of the new temperature measurement system was tested up to 1650ºC. The relationship between the OPD and the temperature is shown in Figure 5.5(a). The calibrated relation can be approximated by the second-order equation:

$$T(^{\circ}C) = -2.7702d^2 - 45.217d + 4719.1 \quad (\text{d in } \mu\text{m}). \qquad \textbf{(5-2)}$$

With this calibration equation, the optical sensor measured temperature values can be obtained through measurements of the OPD. Figure 5.5(b) compares the optical sensor measured temperature with high temperature thermocouple measurement results. A good match was demonstrated, especially at high temperature.

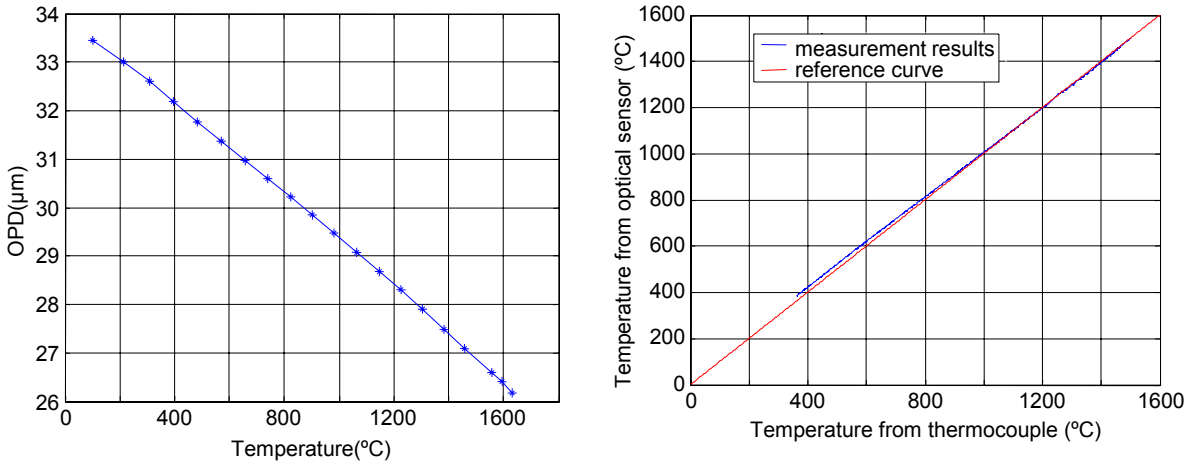

(a) **(b)**

Figure 5.5. Testing results for the newly designed sensor prototype: (a) calibration relationship between temperature and OPD; (b) optical sensor temperature measurements.

6.0 Conclusions and Future Work

The main objective of this project is to bring the BPDI sensor technology, which is already demonstrated in the laboratory, to a level where the sensor can be deployed in the harsh industrial environments and will become commercially viable. Research efforts were thus focused on analyzing and testing the effect of performance degrading factors on the initially demonstrated sensor design. Those factors include optical signal quality and mechanical stability of the sensing probe. Other factors will be analyzed in the future in order to optimize its performance. A new version of the sensing probe was then developed based on a single crystal sapphire right angle prism. The mechanical structure is simplified and the stability of the system increased with this new sensing probe design. This is a major advance in the overall program to scale up the sensor system for a full field demonstration at Global Energy Technology's Wabash River Facility.

With a single crystal sapphire right angle prism as the sensing element, the temperature sensor achieved a wide dynamic range over 1600ºC with high accuracy. Its resolution and accuracy are comparable to commercially available B-type thermocouples. Further resolution improvement can be achieved by changing the sensing element dimensions. The structure of this sensor is simple and cost-effective for high temperature sensing, and is also designed to be robust enough to survive in real engineering environments.

The sensor instrumentation will be designed for continuous operation in an actual coal gasification facility under high temperatures and extremely corrosive conditions. Based on the results shown in this report, future research work will mainly focus on three areas:

1. Further laboratory testing and calibration of the newly revised sensor version

Prior to the field ready prototype for actual installation of the temperature sensor system in the gasification unit, the entire system will be tested in the laboratory to ensure proper operation, which will include updating of the software for the whole system. By employing Visual Basic or LabVIEW; a graphical user interface (GUI) will be used to display the data for inspection and the data will also be stored on the hard disk for further analysis.

2. Field ready sensor prototype design

In conjunction with our industrial collaborator, the requirements for the system and system integration with the existing gasification facility will be outlined. Based upon the requirements, the field test ready prototype system will be designed and fabricated. This task includes the design and fabrication of a protective housing – although the corrosion resistance of the single crystal sapphire material has been documented in laboratory testing, special consideration will be given to the required mechanical protection of both the sensor probe and the associated signal demodulation system.

3. Site preparation and installation

The field test site will be prepared for installation of the sensor system. After all external infrastructure is installed for communication of the signal to an appropriate location, the sensor probe will be installed in the gasifier. The system will be operated for several months to evaluate the performance. The data obtained during the field test will be analyzed to determine the performance of the temperature sensor in the gasification unit.

References

1. Y. Zhang, G. R. Pickrell, B. Qi, R. G. May and A. Wang, Single Crystal Sapphire High Temperature Measurement Instrument for Coal Gasification,*The 8th Symposium on Temperature: Its Measurement and Application in Science and Industry Conference Proceedings* Chicago, pp. (Peer Reviewed) (2002).
2. Y. Zhang, G. R. Pickrell, B. Qi, R. G. May and A. Wang, BPDI based optical temperature sensor for real-time high temperature measurements for the coal gasification process,*Photonics Asia, Advanced Sensor Systems and Applications, Proc. SPIE* Shanghai, vol. 4920, pp. 4920-2 (2002).
3. Y. Zhang, G. R. Pickrell, B. Qi, R. G. May, and A. Wang, "Optical high temperature measurement instrument with single-crystal sapphire for harsh environment," *submitted to J. Lightwave Tech.* (2002).
4. Y. Zhang, G. R. Pickrell, and A. Wang, *Optical Fiber Single Crystal Sapphire High Temperature Sensing Instrument*, Patent Application Filed (2002).
5. B. Qi, G. R. Pickrell, J. Xu, P. Zhang, Y. Duan, W. Peng, Z. Huang, R. G. May, and A. Wang, "High-resolution white light interferometer and its application," *submitted to Applied Optics* (2001).
6. Y. Zhang, G. Pickrell, B. Qi, R. G. May and A. Wang, Single-crystal sapphire high temperature sensing based on broadband polarimetric interferometer,*Sensors for Industry Conference, Proc. IEEE* Rosemont, IL, pp. 303-307 (2001).
7. B. Qi, W. Huo, H. Xiao, and A. Wang, *Novel Data Processing Method for White Light Interferometric Fiber Optic Sensors*, Patent Application Filed (2001).
8. H. Xiao, W. Huo, J. Deng, M. Luo, Z. Wang, R. G. May, and A. Wang, "Fiber optic white light interferometric spectrum signal processing for absolute measurements," *Harsh Environment Sensors II, Proc. SPIE* **3852**, pp. 74-80, Boston (1999).
9. H. Xiao, Y. Xie, J. Deng, R. G. May, and A. Wang, "Absolute sapphire optical fiber interferometric sensors," *Process Monitoring with Optical Fibers and Harsh Environment Sensors, Proc. SPIE* **3538**, pp. 115-121, Boston (1998).
10. H. Xiao, W. Zhao, R. Lockhart, J. Wang, and A. Wang, "Absolute sapphire optical fiber sensor for high-temperature applications," *Sensors and Controls for Advanced Manufacturing, Proc. SPIE* **3201**, pp. 36-42, Pittsburgh (1997).
11. Y. Zhang, G. Pickrell, B. Qi, R. G. May, and A. Wang, "Single-crystal sapphire high temperature sensing based on broadband polarimetric interferometer," *Sensors for Industry Conference, Proc. IEEE*, pp. 303-307 (2001).
12. X. Fang, R. G. May, A. Wang, and R. O. Claus, "A fiber-optic high temperature sensor," *Sens. Act. A* **44**), 19-24 (1994).
13. A. Wang, S. Gollapudi, R. G. May, K. A. Murphy, and R. O. Claus, "Sapphire optical fiber-based interferometer for high temperature environmental applications," *J. Smart Mat. Struct.* **4**), 147-151 (1995).

List of Acronyms and Abbreviations

A/D, analog to digital
APP, Advanced Pressure Products, Inc.
BPDI, broadband polarimetric differential interferometry
CCD, charge couple device
CPT, Center for Photonics Technology
CTE, coefficient of thermal expansion
EFPI, extrinsic Fabry-Perot interferometer
EMI, electromagnetic interference
FWHM, full width half maximum
GPM, gallons per minute
GRIN, graded index
LED, light emitting diode
MMF, multimode fiber
OPD, optical path difference
PC, personal computer
PZT, lead zirconium titanate
SCIIB, self-calibrated interferometric/intensity-based
SLED, superluminescent light emitting diode
SMF, single mode fiber
SNR, signal to noise ratio
VTPL, Virginia Tech Photonics Laboratory (now Center for Photonics Technology)

Appendix: Refraction Angle and Index for the Extraordinary Wave in Single Crystal Sapphire

When light propagates at the interface of air and single crystal sapphire, the refractive index of the extraordinary wave will depend on the incident angle. As shown in the figure, the refraction index is $|OK|$ along angle θ_2 for light with incident angle θ_0. Using Snell's law,

$$\sin^2\theta_0 = |OK|^2 \sin^2\theta_2 , \qquad \textbf{(A-1)}$$

within the half ellipse of (arc –a-b-a), the length of line OK is:

$$\left.\begin{aligned} X_K &= a\cos t \\ Y_K &= b\sin t \end{aligned}\right\}\text{coordinate for K point}$$
$$|OK|^2 = a^2\cos^2 t + b^2\sin^2 t , \qquad \textbf{(A-2)}$$

where t is an intermediate variable with no physical meanings. Using a simple geometrical relationship, the relationship between t and θ_2 is:

$$\tan\theta_2 = \frac{X_K}{Y_K} = \frac{a\cos t}{b\sin t} = \frac{a}{b\tan t} \Rightarrow \tan t = \frac{a}{b\tan\theta_2} , \qquad \textbf{(A-3)}$$

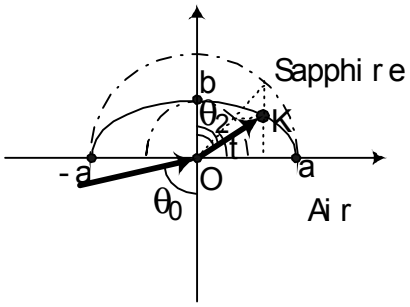

Figure. Refraction at the surface of the air and single crystal sapphire

By putting equation (A-2) and (A-3) into equation (A-1), we have

$$
\begin{aligned}
\sin^2\theta_0 &= (a^2\cos^2 t + b^2\sin^2 t)\sin^2\theta_2 \\
\cdots\cdots &= \frac{a^2 + b^2\tan^2 t}{1+\tan^2 t}\sin^2\theta_2 \\
\cdots\cdots &= \frac{b^2a^2(1+\tan^2\theta_2)}{b^2\tan^2\theta_2 + a^2}\frac{\tan^2\theta_2}{1+\tan^2\theta_2}, \\
\cdots\cdots &= \frac{b^2a^2\tan^2\theta_2}{b^2\tan^2\theta_2 + a^2}
\end{aligned}
\qquad \textbf{(A-4)}
$$

where the following relationships are used.

$$
\left.
\begin{aligned}
\sin^2\beta &= \frac{\tan^2\beta}{1+\tan^2\beta} \\
\cos^2\beta &= \frac{1}{1+\tan^2\beta}
\end{aligned}
\right\} \beta \text{ represents } t \text{ and } \theta_2
\qquad \textbf{(A-5)}
$$

With equation (A-4) and equation (A-2), we have

$$
\begin{aligned}
\theta_2 &= \tan^{-1}\left(\sqrt{\frac{a^2\sin^2\theta_0}{b^2(a^2-\sin^2\theta_0)}}\right) \\
|OK| &= \frac{b^2a^2(1+\tan^2(\theta_2))}{b^2\tan^2(\theta_2)+a^2}
\end{aligned}
, \qquad \textbf{(A-6)}
$$

Relating the index ellipse to refractive index,

$$
\begin{aligned}
a &= n_o \\
b &= n_{eo} \\
|OK| &= n_e
\end{aligned}
, \qquad \textbf{(A-7)}
$$

where n_{eo} is a special n_e value for incident light normal to the surface of the a-plane sapphire disk. By putting equation (7) into equation (6):

$$
\begin{aligned}
\theta_2 &= \tan^{-1}\left(\sqrt{\frac{{n_o}^2\sin^2\theta_0}{{n_{eo}}^2({n_o}^2-\sin^2\theta_0)}}\right) \\
n_e &= \frac{{n_{eo}}^2{n_o}^2(1+\tan^2(\theta_2))}{{n_{eo}}^2\tan^2(\theta_2)+{n_o}^2}
\end{aligned}
. \qquad \textbf{(A-8)}
$$